ELSEVIER

Journal of Fluids and Structures 19 (2004) 557–572

JOURNAL OF FLUIDS AND STRUCTURES

www.elsevier.nl/locate/jnlabr/yjfls

A higher-order-coupled boundary element and finite element method for the wave forcing of a floating elastic plate

C.D. Wang[a], M.H. Meylan[b,*]

[a] *Institute of Information and Mathematical Sciences, Massey University, Albany 102-904 NSMC, Auckland, New Zealand*
[b] *Department of Mathematics, University of Auckland, Private Bag 92019, Auckland, New Zealand*

Received 11 March 2003; accepted 24 February 2004

Abstract

We present a higher-order method to calculate the motion of a floating, shallow draft, elastic plate of arbitrary geometry subject to linear wave forcing at a single frequency. The solution is found by coupling the boundary element and finite element methods. We use the same nodes, basis functions, and maintain the same order in both methods. Two equations are derived that relate the displacement of the plate and the velocity potential under the plate. The first equation is derived from the elastic plate equation. The discrete version of this equation is very similar to the standard finite element method elastic plate equation except that the potential of the water is included in a consistent manner. The second equation is based on the boundary integral equation which relates the displacement of the plate and the potential using the free-surface Green function. The discrete version of this equation, which is consistent with the order of the basis functions, includes a Green matrix that is analogous to the mass and stiffness matrices of the classical finite element method for an elastic plate. The two equations are solved simultaneously to give the potential and displacement. Results are presented showing that the method agrees with previous results and its performance is analysed.

1. Introduction

The floating thin elastic plate of shallow draft can be used to model a range of physical systems, for example ice floes or very large floating structures. It is also of theoretical importance as one of the simplest models of hydroelasticity. It is not surprising therefore that the floating elastic plate has been the subject of significant research. Much of this research, especially that which was motivated by the construction of very large floating structures, is summarized in the review papers by Kashiwagi (2000) and Watanabe et al. (2004). The review paper by Squire et al. (1995) summarizes the research prior to 1995 which was motivated by modelling sea ice floes, but does not include the more recent work, Meylan and Squire (1996) and Meylan (2002), in which the solution for a three-dimensional ice floe is presented.

The linear wave forcing of a floating elastic plate requires that two equations relating the displacement of the plate and the velocity potential of the water (or equivalently the pressure) be solved. We refer to these two equations as the plate and water equations, respectively. There are two basic methods to solve these equations, called the *modal expansion method* and the *direct method*, respectively. In the modal expansion method the plate motion is expanded as a sum of modal functions. Different modal functions have been chosen, the most common being free–free beam modes [e.g. Kashiwagi, (1998)] or the modes of a vibration of a free plate [e.g. Meylan and Squire, (1996); Meylan, (2002)]. In the direct method, the equations are solved directly without expanding the plate motion in modes. The direct method

*Corresponding author.
Email-address: meylan@math.auckland.ac.nz (M.H. Meylan).

0889-9746/$ - see front matter © 2004 Elsevier Ltd. All rights reserved.
doi:10.1016/j.jfluidstructs.2004.02.006

was used by Meylan and Squire (1994), Ohkusu and Namba (1998) and Hermans (2000) in two-dimensions, and Yasuzawa et al. (1996), Yago and Endo (1996), and Hamamoto et al. (1997) in three dimensions, amongst others.

The advantages of the modal expansion method are as follows: the number of unknowns to describe the plate motion is reduced, the rigid body solution method can be used (Bishop et al., 1986) and, if the plate geometry is simple enough, the modes may be calculated trivially, thus removing the need to solve the plate equation numerically. However, for situations where the plate geometry is not regular and where the relative plate stiffness is small, the modal expansion method is no longer preferable. This is because it now becomes numerically challenging to find modes to expand the plate motion that avoid having to solve the plate equation and because the number of modes required becomes large. The situation of low relative plate stiffness and irregular shape is particularly applicable to modelling ice floes.

It is generally agreed that the finite element method (FEM) is the best method to solve the plate equation (for anything but the simplest plate geometries) while the boundary element method (BEM) is best suited to solve the water equation. For this reason, Yasuzawa et al. (1996), Yago and Endo (1996), and Hamamoto et al. (1997) developed hybrid FEM-BEM methods in which the same unknowns were used in the FEM and the BEM. However, they did not use the same modal functions for the FEM and the BEM so that the order of the BEM was lower than that used in the FEM. It is well recognized that there are advantages to solving the BEM equation using a higher-order method, especially for short wavelengths. This is the reason why a higher-order method is used in Kashiwagi (1998).

In this paper, we will derive a higher-order FEM–BEM method for the floating elastic plate in which the same unknowns (nodes) and basis functions are used in both the FEM and the BEM. This differs from the higher-order method presented by Kashiwagi (1998) where different basis functions for the plate and water velocity potential, neither of which were the FEM basis functions, were used. We present some results for various plate geometries and properties. We establish that the results agree with those given in Meylan (2002) and we show that the performance of the present method is much better than the low-order method which was used there. We also establish convergence tests for the number of points used to integrate the boundary element equations. We then present some displacement results for four different geometries.

2. The equations of motion

In this section, we will derive two coupled equations, one from the equation of motion for an elastic plate and the other from the linear water wave equation, which govern the motion of a floating elastic plate of shallow draft subject to linear wave forcing. Fig. 1 is a schematic diagram showing the coordinate system and some of the equations of motion. The vertical coordinate, z points upwards, with the water surface at $z = 0$ and the sea floor at $z = -H$ (or $z = -\infty$ for infinitely deep water). The horizontal coordinates are x and y and we denote the pair (x, y) by the vector $\mathbf{x}$. The plate floats on the water surface with negligible draft. We will begin by considering the equations for the elastic plate.

2.1. The elastic plate equation

The plate is assumed to be thin, elastic, to float on the water surface with zero-draft, and to be of arbitrary shape. The equation of motion for the plate is given by the elastic plate equation,

$$D\nabla^4 W + \rho_i h \frac{\partial^2 W}{\partial t^2} = p \tag{1}$$

together with the boundary conditions

$$\frac{\partial^2 W}{\partial n^2} + \nu \frac{\partial^2 W}{\partial s^2} = 0 \quad \text{and} \quad \frac{\partial^3 W}{\partial n^3} + (2 - \nu) \frac{\partial^3 W}{\partial s^3} = 0 \tag{2}$$

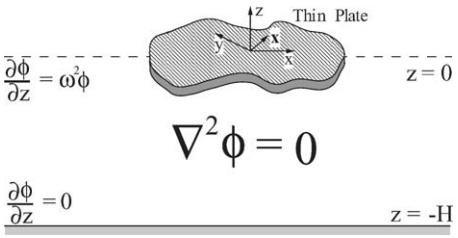

Fig. 1. A schematic diagram showing the coordinates used in the solution and the equations of motion for the water.

(Hildebrand, 1965) where $W(x,y,t)$ is the plate displacement, D is the rigidity constant of the plate, ρ_i is the plate density, h is the plate's thickness, p is the pressure at the water surface, v is Poisson's ratio, and n and s denote the normal and tangential directions respectively. We assume that the pressure at the water surface is given by the linearized Bernoulli's equation,

$$p = -\rho \left.\frac{\partial \Phi}{\partial t}\right|_{z=0} - \rho g W, \tag{3}$$

where $\Phi(x,y,z,t)$ is the velocity potential of the water, ρ is the density of the water, and g is the gravitational acceleration constant. Note that $W(x,y,t)$ is independent of z whereas $\Phi(x,y,z,t)$ is z-dependent. Equating (1) and (3) gives us

$$D\nabla^4 W + \rho_i h \frac{\partial^2 W}{\partial t^2} = -\rho \left.\frac{\partial \Phi}{\partial t}\right|_{z=0} - \rho g W. \tag{4}$$

2.1.1. Nondimensionalizing the variables

We nondimensionalize the spatial variables with respect to a length parameter L (for example, L may be derived from the area of the plate or L may be the characteristic length $(D/\rho g)^{1/4}$) and the time variables with respect to $\sqrt{L/g}$. The dimensionless variables are therefore given by

$$\bar{x} = \frac{x}{L}, \quad \bar{y} = \frac{y}{L}, \quad \bar{z} = \frac{z}{L}, \quad \bar{W} = \frac{W}{L}, \quad \bar{t} = t\sqrt{\frac{g}{L}} \text{ and } \bar{\Phi} = \frac{\Phi}{L\sqrt{Lg}}.$$

Using the dimensionless variables Eq. (4) becomes

$$\beta\nabla^4 \bar{W} + \gamma \frac{\partial^2 \bar{W}}{\partial \bar{t}^2} = -\left.\frac{\partial \bar{\Phi}}{\partial \bar{t}}\right|_{z=0} - \bar{W}, \tag{5}$$

where the constants β and γ are given by

$$\beta = \frac{D}{\rho L^4 g} \quad \text{and} \quad \gamma = \frac{\rho_i h}{\rho L}.$$

We will refer to β as the *stiffness* constant and γ as the *mass* constant. This notation is based on Tayler (1986).

2.1.2. The single frequency equations

We will consider the solution for a single frequency and we can therefore represent the displacement and the potential as the real parts of complex functions in which the time dependence is $e^{-i\omega t}$ where ω is the dimensionless radian frequency, i.e.

$$\bar{W}(\bar{x},\bar{y},\bar{t}) = Re[w(\bar{x},\bar{y})e^{-i\omega\bar{t}}],$$

$$\bar{\Phi}(\bar{x},\bar{y},\bar{z},\bar{t})|_{z=0} = Re[\phi(\bar{x},\bar{y})e^{-i\omega\bar{t}}].$$

Therefore Eq. (5) becomes

$$\beta\nabla^4 w(\bar{x},\bar{y}) - \omega^2\gamma\omega(\bar{x},\bar{y}) = i\omega\phi(\bar{x},\bar{y}) - w(\bar{x},\bar{y}), \tag{6}$$

which we will refer to as the *plate equation*. For reasons of clarity, in what follows we will omit the overbar from the dimensionless variables.

2.2. Equations of motion for the water

We consider water of infinite depth or finite depth H. The velocity potential for the water is assumed to satisfy Laplace's equation together with the appropriate linearized boundary conditions given by

$$\nabla^2\phi = 0, \quad -\infty < z < 0,$$

$$\frac{\partial \phi}{\partial z} = 0, \quad z = -H \text{ or } z = -\infty,$$

$$\frac{\partial \phi}{\partial z} = -\mathrm{i}\omega w, \quad z = 0, \ \mathbf{x} \in \Delta,$$
$$\frac{\partial \phi}{\partial z} - \omega^2 \phi = 0, \ z = 0, \ \mathbf{x} \notin \Delta, \tag{7}$$

where Δ is region of the water surface which is covered by the plate. The velocity potential is also subject to the Sommerfeld radiation condition as $|\mathbf{x}| \to \infty$,

$$\lim_{|\mathbf{x}| \to \infty} \sqrt{|\mathbf{x}|}\left(\frac{\partial}{\partial |\mathbf{x}|} - \mathrm{i}\omega^2\right)(\phi - \phi^{in}) = 0 \tag{8}$$

(Wehausen and Laitone, 1960), where ϕ^{in} is the incident potential. We assume that the incident potential is a plane wave given by

$$\phi^{in} = \frac{A}{\omega} \mathrm{e}^{\mathrm{i}k(x \cos\theta + y \sin\theta)} \mathrm{e}^{kz} \tag{9}$$

for infinite depth and

$$\phi^{in} = \frac{A}{\omega} \mathrm{e}^{\mathrm{i}k(x \cos\theta + y \sin\theta)} \frac{\cosh k(z+H)}{\cosh kH} \tag{10}$$

for finite depth. In Eqs. (9) and (10) A is the dimensionless amplitude, k is the wavenumber (the wavelength $\lambda = 2\pi/k$), which is ω^2 in infinite depth and the positive real solution of the nondimensional dispersion equation

$$k \tanh kH = \omega^2$$

in finite depth, and θ is the direction of propagation of the wave. We transform the linear wave potential problem given by Eq. (7) with boundary condition (8) to an integral equation using the free-surface Green function (Wehausen and Laitone, 1960; Kashiwagi, 2000). The free-surface Green function, $G(\mathbf{x}; \xi)$, satisfies

$$\nabla^2_{\mathbf{x}} G = 0,$$
$$\frac{\partial G}{\partial z} - \omega^2 G = -\delta(\mathbf{x} - \xi), \quad z = 0,$$
$$\frac{\partial G}{\partial z} = 0, \quad z = -H \ \text{or} \ z = -\infty,$$

where $\xi = (\xi, \eta)$. This gives us

$$\phi(\mathbf{x}) = \phi^{in} + \int_{\Delta} G(\mathbf{x}; \xi)(\omega^2 \phi(\xi) + \mathrm{i}\omega w(\xi)) \, \mathrm{d}S_{\xi}, \tag{11}$$

where the kernel of the integral operator is the free-surface Green function and we restrict ϕ^{in} to $z = 0$. The free-surface Green function can be found by taking the limit as the source and field points tend to $z = 0$ of the three-dimensional Green function whose Laplacian is equal to the delta function in the fluid and which satisfies the zero condition on the free surface. The free-surface Green function is given by

$$G(\mathbf{x}; \xi) = -\frac{1}{4\pi}\left(\frac{2}{|\mathbf{x} - \xi|} - \pi\omega^2[\mathrm{H}_0(\omega^2|\mathbf{x} - \xi|) + \mathrm{Y}_0(\omega^2|\mathbf{x} - \xi|) - 2\mathrm{i}\pi \mathrm{J}_0(\omega^2|\mathbf{x} - \xi|)]\right) \tag{12}$$

for infinite depth (Kim, 1965) and

$$G(\mathbf{x}; \xi) = -\frac{\mathrm{i}}{2}\frac{\omega^4 - k^2}{(\omega^4 - k^2)H - \omega^2}\cosh^2(kH)\mathrm{H}_0^{(1)}(k|\mathbf{x} - \xi|) - \frac{1}{\pi}\sum_{m=1}^{\infty}\frac{k_m^2 + \omega^4}{(k_m^2 + \omega^4)H - \omega^2}\cos^2(k_m H)\mathrm{K}_0(k_m|\mathbf{x} - \xi|) \tag{13}$$

for finite depth (John, 1950). The values of k_m, $m > 0$, are the positive real roots of the dispersion equation

$$\omega^2 + k_m \tan k_m d = 0. \tag{14}$$

In Eqs. (12) and (13) J_0 and Y_0 are Bessel functions of the first kind and second kind of order zero, respectively, K_0 is a modified Bessel function of the second kind of order zero, $\mathrm{H}_0^{(1)}$ is a Hankel Function of order zero, and H_0 is the Struve function of order zero (Abramowitz and Stegun, 1970). Note that G depends only on $|\mathbf{x} - \xi|$, however there is a singularity when $\mathbf{x} = \xi$.

By expressing the integral operator in Eq. (11) as

$$\mathbf{G}f(\mathbf{x}) = \int_{\Delta} G(\mathbf{x};\xi) f(\xi)\,\mathrm{d}\xi$$

it can be written as

$$\phi(\mathbf{x}) = \phi^{in}(\mathbf{x}) + \omega^2 \mathbf{G}\phi(\mathbf{x}) + \mathrm{i}\omega\,\mathbf{G}w(\mathbf{x}), \tag{15}$$

which we will refer to as the *water equation*. The plate Eq. (6) and the water Eq. (15) must be solved simultaneously.

3. Discrete versions of the plate and water equations

In this section, we will derive discrete versions of the plate Eq. (6) and the water Eq. (15). We will use the finite element method (FEM) to solve the plate equation and the boundary element method (BEM) to solve the water equation. The same basis functions will be used in both methods.

3.1. Expansion of the displacement and potential

We will present the details of how we expand the displacement and potential using the finite element basis functions. The basis functions will be defined over square panels, but our method could be generalized straightforwardly to other FEM basis functions. We discretize the plate by dividing it into a finite number of p uniform square panels of area $4a^2$. We denote each panel by Δ_d where $1 \leqslant d \leqslant p$. Each panel consists of four nodes at the edges and each node has three degrees of freedom. The three degrees of freedom are the displacement (w) and its two derivatives ($\partial w/\partial x$ and $\partial w/\partial y$). Fig. 2 shows a schematic diagram for a panel. Within the panel the local index of the nodes is 1, 2, 3, and 4 as shown. The global index of the nodes for a particular panel Δ_d are $q_1^{(d)}$, $q_2^{(d)}$, $q_3^{(d)}$, and $q_4^{(d)}$, again as shown. We always number the nodes in such a way that $q_2^{(d)} = q_1^{(d)} + 1$ and $q_4^{(d)} = q_3^{(d)} + 1$. The total number of nodes in the plate is q.

We use nonconforming square elements (Petyt, 1990) to expand the plate motion. Assuming that $\mathbf{x} \in \Delta_d$ we use the standard FEM to approximate $w(\mathbf{x})$ at Δ_d. The displacement $w(\mathbf{x})$ is represented as a product of a vector of functions which depend on $\mathbf{x}$ and a constant vector,

$$w(\mathbf{x}) = \mathbf{N}_d(\mathbf{x})\hat{\mathbf{w}}_d, \quad \mathbf{x} \in \Delta_d, \tag{16}$$

where $\mathbf{N}_d(\mathbf{x})$ is the vector of basis functions, which we will call the *basis vector*. The basis vector is defined by

$$\mathbf{N}_d(\mathbf{x}) = [N_{11}\ N_{12}\ N_{13}\ N_{21}\ N_{22}\ N_{23}\ N_{31}\ N_{32}\ N_{33}\ N_{41}\ N_{42}\ N_{43}], \tag{17}$$

where $N_{j1} = N_{j1}(\hat{x},\hat{y})$, $N_{j2} = N_{j2}(\hat{x},\hat{y})$, and $N_{j3} = N_{j3}(\hat{x},\hat{y})$ ($j = 1, 2, 3, 4$) are given by

$$\begin{aligned}
N_{j1}(\hat{x},\hat{y}) &= \frac{1}{8}(1+\hat{x}_j\hat{x})(1+\hat{y}_j\hat{y})(2+\hat{x}_j\hat{x}+\hat{y}_j\hat{y}-\hat{x}^2-\hat{y}^2),\\
N_{j2}(\hat{x},\hat{y}) &= \frac{a}{16}(1+\hat{x}_j\hat{x})(\hat{y}_j+\hat{y})(\hat{y}^2-1),\\
N_{j3}(\hat{x},\hat{y}) &= -\frac{a}{16}(\hat{x}_j+\hat{x})(\hat{x}^2-1)(1+\hat{y}_j\hat{y}).
\end{aligned} \tag{18}$$

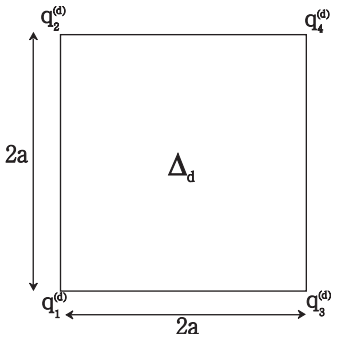

Fig. 2. Diagram of square panel Δ_d showing the numbering of the nodes.

The pair $(\hat{x},\hat{y})$ is $(x/a, y/a)\in\Delta_d$ and $-1\leqslant\hat{x}_j,\ \hat{y}_j\leqslant 1$ where j denotes the jth node of Δ_d. The vector $\hat{\mathbf{w}}_d$ is a vector of constants, which is given by

$$\hat{\mathbf{w}}_d = \left[w_1^{(d)} \ \frac{\partial w_1^{(d)}}{\partial x} \ \frac{\partial w_1^{(d)}}{\partial y} \ w_2^{(d)} \ \frac{\partial w_2^{(d)}}{\partial x} \ \frac{\partial w_2^{(d)}}{\partial y} \ w_3^{(d)} \ \frac{\partial w_3^{(d)}}{\partial x} \ \frac{\partial w_3^{(d)}}{\partial y} \ w_4^{(d)} \ \frac{\partial w_4^{(d)}}{\partial x} \ \frac{\partial w_4^{(d)}}{\partial y} \right]^{\mathrm{T}}, \tag{19}$$

where

$$w_j^{(d)} = w(\mathbf{x}_j), \quad \frac{\partial w_j^{(d)}}{\partial x} = \frac{\partial}{\partial x} w(\mathbf{x}_j), \quad \frac{\partial w_j^{(d)}}{\partial y} = \frac{\partial}{\partial y} w(\mathbf{x}_j)$$

and $\mathbf{x}_j\in\Delta_d$. The basis vector $\mathbf{N}_d$ is of dimension 1×12 and the constant vector $\hat{\mathbf{w}}_d$ has dimension 12×1.

We expand the potential in an identical manner to the displacement, i.e.,

$$\phi(\mathbf{x}) = \mathbf{N}_d(\mathbf{x})\hat{\phi}_d, \quad \mathbf{x}\in\Delta_d, \tag{20}$$

where $\hat{\phi}_d$ is the vector of constants defined by the following:

$$\hat{\phi}_d = \left[\phi_1^{(d)} \ \frac{\partial \phi_1^{(d)}}{\partial x} \ \frac{\partial \phi_1^{(d)}}{\partial y} \ \phi_2^{(d)} \ \frac{\partial \phi_2^{(d)}}{\partial x} \ \frac{\partial \phi_2^{(d)}}{\partial y} \ \phi_3^{(d)} \ \frac{\partial \phi_3^{(d)}}{\partial x} \ \frac{\partial \phi_3^{(d)}}{\partial y} \ \phi_4^{(d)} \ \frac{\partial \phi_4^{(d)}}{\partial x} \ \frac{\partial \phi_4^{(d)}}{\partial y} \right]^{\mathrm{T}}$$

and

$$\phi_j^{(d)} = \phi(\mathbf{x}_j), \quad \frac{\partial \phi_j^{(d)}}{\partial x} = \frac{\partial}{\partial x}\phi(\mathbf{x}_j) \ \text{ and } \ \frac{\partial \phi_j^{(d)}}{\partial y} = \frac{\partial}{\partial y}\phi(\mathbf{x}_j).$$

Likewise $\phi^{in}(\mathbf{x})$ can be written as

$$\phi^{in}(\mathbf{x}) = \mathbf{N}_d(\mathbf{x})\hat{\phi}_d^{in}, \tag{21}$$

where

$$\hat{\phi}_d^{in} = \left[\phi_1^{in} \ \frac{\partial \phi_1^{in}}{\partial x} \ \frac{\partial \phi_1^{in}}{\partial y} \ \phi_2^{in} \ \frac{\partial \phi_2^{in}}{\partial x} \ \frac{\partial \phi_2^{in}}{\partial y} \ \phi_3^{in} \ \frac{\partial \phi_3^{in}}{\partial x} \ \frac{\partial \phi_3^{in}}{\partial y} \ \phi_4^{in} \ \frac{\partial \phi_4^{in}}{\partial x} \ \frac{\partial \phi_4^{in}}{\partial y} \right]^{\mathrm{T}}$$

and

$$\phi_j^{in} = \phi^{in}(\mathbf{x}_j), \quad \frac{\partial \phi_j^{in}}{\partial x} = \frac{\partial}{\partial x}\phi^{in}(\mathbf{x}_j), \quad \frac{\partial \phi_j^{in}}{\partial y} = \frac{\partial}{\partial y}\phi^{in}(\mathbf{x}_j),$$

$\mathbf{x}_j\in\Delta_d$ and ϕ^{in} is given by Eq. (9).

3.2. The plate equation

We will solve the plate Eq. (6) using the representation of the potential and displacement in the finite element basis functions. We reduce Eq. (6) defined for the entire plate to an equivalent equation that is applicable only to a panel by considering $\mathbf{x}\in\Delta_d$. We apply (16) and (20) to replace $w(\mathbf{x})$ and $\phi(\mathbf{x})$ in (6) to obtain

$$\beta\nabla^4(\mathbf{N}_d\hat{\mathbf{w}}_d) - \omega^2\gamma(\mathbf{N}_d\hat{\mathbf{w}}_d) = \mathrm{i}\omega(\mathbf{N}_d\hat{\phi}_d) - (\mathbf{N}_d\hat{\mathbf{w}}_d).$$

We transform (6) into its variational and minimize respect to $\hat{\mathbf{w}}_d$ to obtain

$$\int_{\Delta_d}\left\{\beta\left[\frac{\partial^2\mathbf{N}_d^{\mathrm{T}}}{\partial x^2}\frac{\partial^2\mathbf{N}_d}{\partial x^2} + \frac{\partial^2\mathbf{N}_d^{\mathrm{T}}}{\partial y^2}\frac{\partial^2\mathbf{N}_d}{\partial y^2} + 2(1-\nu)\frac{\partial^2\mathbf{N}_d^{\mathrm{T}}}{\partial x\partial y}\frac{\partial^2\mathbf{N}_d}{\partial x\partial y} + 2\nu\frac{\partial^2\mathbf{N}_d}{\partial x^2}\frac{\partial^2\mathbf{N}_d}{\partial y^2}\right]\right\}\mathrm{d}\mathbf{x}^{(d)}\hat{\mathbf{w}}_d$$
$$-\int_{\Delta_d}\{\omega^2\gamma\mathbf{N}_d^{\mathrm{T}}\mathbf{N}_d\}\,\mathrm{d}\mathbf{x}^{(d)}\hat{\mathbf{w}}_d = \int_{\Delta_d}[\mathrm{i}\omega\mathbf{N}_d^{\mathrm{T}}\mathbf{N}_d\hat{\phi}_d - \mathbf{N}_d^{\mathrm{T}}\mathbf{N}_d\hat{\mathbf{w}}_d]\,\mathrm{d}\mathbf{x}^{(d)} \tag{22}$$

(Meylan, 2001). We now introduce the notation

$$\langle\mathbf{N}_d,\mathbf{N}_d\rangle_{\Delta_d} = [m]_d, \tag{23}$$

where the inner product is defined to be the integral over Δ_d, i.e.

$$\langle\mathbf{N}_d,\mathbf{N}_d\rangle_{\Delta_d} = \int_{\Delta_d}\mathbf{N}_d^{\mathrm{T}}\mathbf{N}_d\,\mathrm{d}\mathbf{x}^{(d)} \tag{24}$$

and $[m]_d$ is called the *mass matrix* for the panel Δ_d in the standard FEM terminology and

$$\int_{\Delta_d}\left[\frac{\partial^2\mathbf{N}_d^{\mathrm{T}}}{\partial x^2}\frac{\partial^2\mathbf{N}_d}{\partial x^2}+\frac{\partial^2\mathbf{N}_d^{\mathrm{T}}}{\partial y^2}\frac{\partial^2\mathbf{N}_d}{\partial y^2}+2(1-\nu)\frac{\partial^2\mathbf{N}_d^{\mathrm{T}}}{\partial x\partial y}\frac{\partial^2\mathbf{N}_d}{\partial x\partial y}+2\nu\frac{\partial^2\mathbf{N}_d}{\partial x^2}\frac{\partial^2\mathbf{N}_d}{\partial y^2}\right]\mathrm{d}\mathbf{x}^{(d)}=[k]_d, \tag{25}$$

where $[k]_d$ is called the *stiffness matrix* for the panel Δ_d in the standard FEM terminology (Petyt, 1990).

By substituting the mass matrix from (23) and the stiffness matrix from (25) into (22) we obtain

$$\beta[k]_d\hat{\mathbf{w}}_d-\omega^2\gamma[m]_d\hat{\mathbf{w}}_d=\mathrm{i}\omega[m]_d\hat{\phi}_d-[m]_d\hat{\mathbf{w}}_d, \tag{26}$$

which is the discrete version of the plate Eq. (6) for a single panel.

3.3. Solution of the water equation

We will now solve the water Eq. (15) using the representation of the displacement and potential in the finite element basis functions. Substituting (20) and (21) into (15) we obtain

$$\mathbf{N}_d(\mathbf{x})\hat{\phi}_d=\mathbf{N}_d\hat{\phi}_d^{in}+\omega^2\sum_{e=1}^{p}(\mathbf{G}_{de}\mathbf{N}_e)\hat{\phi}_e+\mathrm{i}\omega\sum_{e=1}^{p}(\mathbf{G}_{de}\mathbf{N}_e)\hat{\mathbf{w}}_e,\quad \mathbf{x}\in\Delta_d, \tag{27}$$

where

$$\mathbf{G}_{de}\mathbf{N}_e=\int_{\Delta_e}G(\mathbf{x};\xi)\mathbf{N}_e(\xi)\,\mathrm{d}\xi. \tag{28}$$

We apply an inner product with $\mathbf{N}_d$ to both sides of (27). This gives us

$$\langle\mathbf{N}_d,\mathbf{N}_d\rangle_{\Delta_d}\hat{\phi}_d=\langle\mathbf{N}_d,\mathbf{N}_d\rangle_{\Delta_d}\hat{\phi}_d^{in}+\omega^2\sum_{e=1}^{p}\langle\mathbf{N}_d,(\mathbf{G}_{de}\mathbf{N}_e)\rangle_{\Delta_d}\hat{\phi}_e+\mathrm{i}\omega\sum_{e=1}^{p}\langle\mathbf{N}_d,(\mathbf{G}_{de}\mathbf{N}_e)\rangle_{\Delta_d}\hat{\mathbf{w}}_e, \tag{29}$$

where

$$\langle\mathbf{N}_d,(\mathbf{G}_{de}\mathbf{N}_e)\rangle_{\Delta_d}=\int_{\Delta_d}\mathbf{N}_d^{\mathrm{T}}\mathbf{G}_{de}\mathbf{N}_e\,\mathrm{d}\mathbf{x}^{(d)}. \tag{30}$$

Analogous to the definitions of the mass and stiffness matrix, we define

$$\int_{\Delta_d}\mathbf{N}_d^{\mathrm{T}}(\mathbf{G}_{de}\mathbf{N}_e)\,\mathrm{d}\mathbf{x}^{(d)}=[g]_{de}, \tag{31}$$

where we call $[g]_{de}$ the *Green matrix*. The numerical calculation of $[g]_{de}$ will be discussed in the next section.

Therefore Eq. (29) for a panel Δ_d is given by

$$[m]_d\hat{\phi}_d=[m]_d\hat{\phi}_d^{in}+\omega^2\sum_{e=1}^{p}[g]_{de}\hat{\phi}_e+\mathrm{i}\omega\sum_{e=1}^{p}[g]_{de}\ \hat{\mathbf{w}}_e, \tag{32}$$

which is the discrete version of the water Eq. (15) for a single panel.

4. Calculating the Green matrix

In this section, we will present the method used to calculate the Green matrix given by Eq. (31). The calculation of this matrix is the principle numerical difficulty in our solution method. The calculation of $[g]_{de}$ will be separated into two cases depending on whether $d=e$ or not. This is because the free-surface Green function (12) is singular at $|\mathbf{x}-\xi|=0$. Since $\mathbf{x}$ lies in panel d and ξ lies in panel e the singularity only occurs when $d=e$. We also notice from (31) that the Green function occurs only in the integral equation $\mathbf{G}_{de}\mathbf{N}_e$ and therefore we need only separate the solution $\mathbf{G}_{de}\mathbf{N}_e$ into the singular and the non singular cases.

The integral equation $\mathbf{G}_{de}\mathbf{N}_e$ can be solved using an elementary numerical integration method. This is done by approximating the integral in the following way:

$$\begin{aligned}\mathbf{G}_{de}\mathbf{N}_e &= \int_{\Delta_e} G(\mathbf{x};\xi)\mathbf{N}_e(\xi)\,\mathrm{d}\xi,\\ &= \sum_{j=1}^{M} v_j G(\mathbf{x};\xi_j)\mathbf{N}_e(\xi_j), \quad \mathbf{x}\in\Delta_d,\ \xi_j\in\Delta_e,\end{aligned} \tag{33}$$

where ξ_j and v_j are sets of M integration points and their corresponding weights over Δ_e. The integral in Eq. (31) will be calculated using a similar numerical scheme, with the possibility of choosing different points and weights given by

$$\int_{\Delta_d} \mathbf{N}_d^{\mathrm{T}}(\mathbf{G}_{de}\mathbf{N}_e)\,\mathrm{d}\mathbf{x}^{(d)} = \sum_{i=1}^{N} u_i \mathbf{N}_d^{\mathrm{T}}(\mathbf{x}_i)(\mathbf{G}_{de}\mathbf{N}_e), \quad \mathbf{x}_i\in\Delta_d, \tag{34}$$

where $\mathbf{x}_i$, and u_i are sets of N integration points and their corresponding weights over Δ_d. Combining (33) and (34) the numerical solution for the Green matrix $[g]_{de}$ is

$$[g]_{de} = \sum_{i=1}^{N} u_i \mathbf{N}_d^{\mathrm{T}}(\mathbf{x}_i) \sum_{j=1}^{M} v_j G^{(ij)} \mathbf{N}_e(\xi_j), \tag{35}$$

where $\mathbf{x}_i\in\Delta_d$, $\xi_j\in\Delta_e$, and $G^{(ij)} = G(\mathbf{x}_i;\xi_j)$.

For the case where $d = e$ we have to solve Eq. (35) using sets of distinct integration points $\{\mathbf{x}_i\}$ and $\{\xi_j\}$ and, hence, distinct $\{u_i\}$ and $\{v_j\}$. This is done to avoid the singularity that occurs whenever $\mathbf{x}_i$ coincides with ξ_j. Also, because of the singularity, we will use more integration points to calculate $\mathbf{G}_{de}\mathbf{N}_e$ when $d = e$. There are other methods which can be used to calculate the singular integral, most notably a coordinate transformation method which is described in Hamamoto et al. (1997). We do not adopt this method here for simplicity but there is not reason why the coordinate transformation method could not be employed with our formulation. For the case where the Green function is not singular (i.e. $d\neq e$) we employ the same set of integration points and their corresponding weights for (34 and (35)). Therefore (35) can be written as

$$[g]_{de} = \begin{cases} \mathbb{N}_1\mathbb{G}_1\mathbb{N}_2 & \text{if } d = e,\\ \mathbb{N}_1\mathbb{G}_2\mathbb{N}_1^{\mathrm{T}} & \text{if } d\neq e,\end{cases} \tag{36}$$

where $\mathbb{G}_1$ is an $N\times M$ rectangular matrix of the form

$$\mathbb{G}_1 = \begin{bmatrix} G^{(11)} & G^{(12)} & \cdots & G^{(1M)}\\ G^{(21)} & G^{(22)} & & \\ & & \ddots & \\ G^{(N1)} & & & G^{(NM)}\end{bmatrix} \tag{37}$$

and $\mathbb{G}_2$ is an $N\times N$ square matrix of the form

$$\mathbb{G}_2 = \begin{bmatrix} G^{(11)} & G^{(12)} & \cdots & G^{(1N)}\\ G^{(21)} & G^{(22)} & & \\ & & \ddots & \\ G^{(N1)} & & & G^{(NN)}\end{bmatrix}. \tag{38}$$

The matrix $\mathbb{N}_1$ is a $12\times N$ matrix of the form

$$\mathbb{N}_1 = [u_1\mathbf{N}_d^{(1)\mathrm{T}} \quad u_2\mathbf{N}_d^{(2)\mathrm{T}} \quad \cdots \quad u_N\mathbf{N}_d^{(N)\mathrm{T}}]$$

and the matrix $\mathbb{N}_2$ is a $M\times 12$ of the form

$$\mathbb{N}_2 = \begin{bmatrix} v_1\mathbf{N}_d^{(1)}\\ v_2\mathbf{N}_d^{(2)}\\ \vdots\\ v_3\mathbf{N}_d^{(M)}\end{bmatrix}.$$

5. Solution of the equations for the entire plate

We have determined the discrete versions of the plate an water equations for each panel. We must now combine these equations so that they apply for the entire plate. Since we are using a set of uniform panels to discretize the plate, the mass matrix (23) and the stiffness matrix (25) are calculated once only. Using a transformation matrix $[o]_d$ we assemble them into the global stiffness and the global mass matrices for the plate

$$\mathbb{K} = \sum_{d=1}^{p} [o]_d^{\mathrm{T}} [k]_d [o]_d, \tag{39}$$

$$\mathbb{M} = \sum_{d=1}^{p} [o]_d^{\mathrm{T}} [m]_d [o]_d, \tag{40}$$

where

$$[o]_d = \begin{bmatrix} & \overbrace{1\ 0\ 0}^{3q_1-2\cdots 3q_1} & & & & & & & \\ \cdots & 0\ 1\ 0 & & & & & & & \\ & 0\ 0\ 1 & & & & & & & \\ & & \overbrace{1\ 0\ 0}^{3q_2-2\cdots 3q_2} & & & & & & \\ & & 0\ 1\ 0 & \cdots & & & & & \\ & & 0\ 0\ 1 & & & & & & \\ & & & & \overbrace{1\ 0\ 0}^{3q_3-2\cdots 3q_3} & & & & \\ & & & \cdots & 0\ 1\ 0 & & & & \\ & & & & 0\ 0\ 1 & & & & \\ & & & & & & \overbrace{1\ 0\ 0}^{3q_4-2\cdots 3q_4} & & \\ & & & & & & 0\ 1\ 0 & \cdots & \\ & & & & & & 0\ 0\ 1 & & \end{bmatrix}, \tag{41}$$

q_j is the index of the jth node of Δ_d and all other entries are zero. It should be noted that, in practice, the sparseness of the matrix $[o]_d$ should be exploited in all calculations. Each transformation matrix $[o]_d$ has the dimension $12 \times 3q$ where q is the total number of nodes in the plate.

We assemble the discrete plate equation for a panel (26) into the discrete plate equation for the entire plate

$$\beta \mathbb{K}\hat{\mathbf{w}} - \omega^2 \gamma \mathbb{M}\hat{\mathbf{w}} = \mathrm{i}\omega \mathbb{M}\hat{\phi} - \mathbb{M}\hat{\mathbf{w}}, \tag{42}$$

where the vectors $\hat{\phi}$ and $\hat{\mathbf{w}}$ are related to $\hat{\mathbf{w}}_d$ and $\hat{\phi}_d$ of Δ_d by

$$\hat{\mathbf{w}}_d = [o]_d \hat{\mathbf{w}}, \tag{43}$$

$$\hat{\phi}_d = [o]_d \hat{\phi}. \tag{44}$$

The discrete water equation for a panel is assembled into the discrete water equation for the plate by applying the transformation matrix $[o]_d$ (41) to (32) to obtain

$$\mathbb{M}\hat{\phi} = \mathbb{M}\hat{\phi}^{in} + \omega^2 \mathbb{G}\hat{\phi} + \mathrm{i}\omega \mathbb{G}\hat{\mathbf{w}}, \tag{45}$$

where

$$\mathbb{G} = \sum_{d=1}^{p} \sum_{e=1}^{p} [o]_d^{\mathrm{T}} [g]_{de} [o]_e \tag{46}$$

is the global Green matrix for the plate. Eq. (42) is solved simultaneously with (45) to obtain $\hat{\mathbf{w}}$ and $\hat{\phi}$.

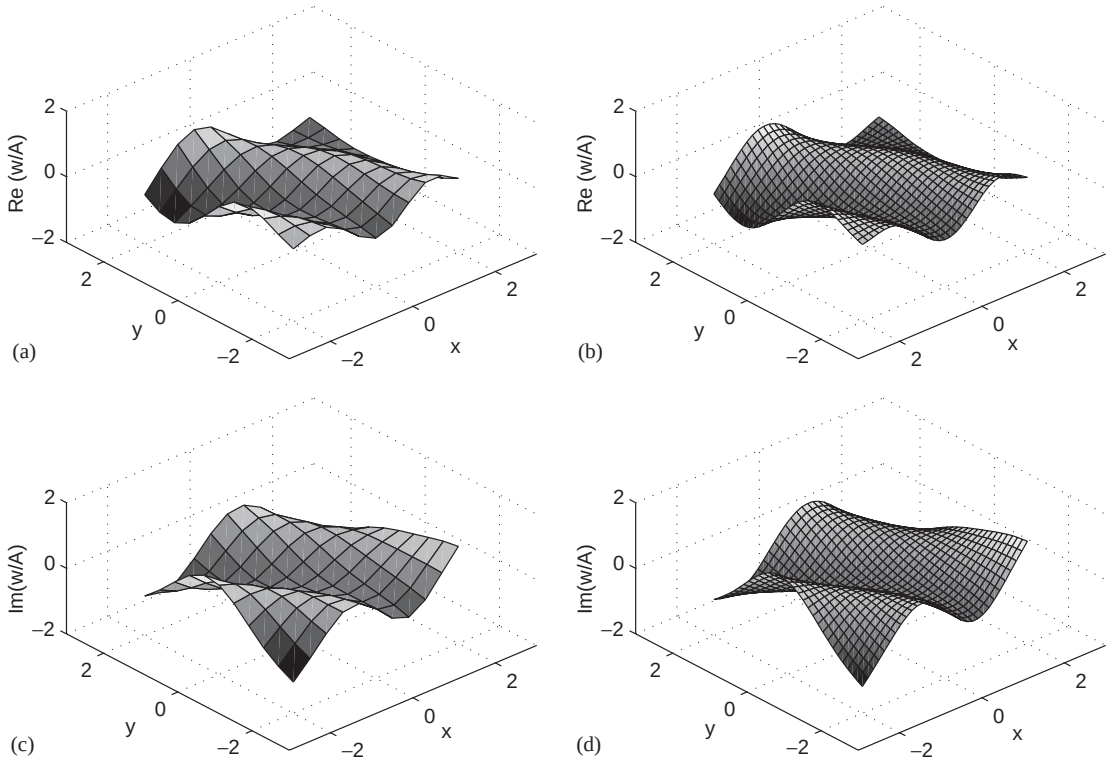

Fig. 3. The comparison of the plate displacement (real and imaginary components) computed using the high-order method (left-hand side) and the low-order method (right-hand side). The stiffness is $\beta = 0.01$, the mass is $\gamma = 0$ and the wave-number is $\omega^2 = \pi$. The wave is incident from the $\theta = \pi/6$ direction.

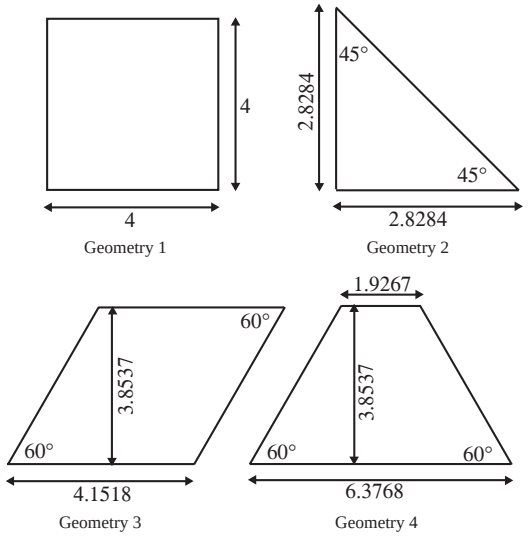

Fig. 4. Diagram of the four geometries of plate shape for which we will calculate solutions.

Having solved for the plate displacement (or the potential) in the FEM basis functions we can recover it as a function of $\mathbf{x}$ using the formula

$$w(\mathbf{x}) = \mathbf{B}(\mathbf{x})\hat{\mathbf{w}},$$

where for $\mathbf{x} \in \Delta_d$

$$\mathbf{B}(\mathbf{x}) = \left[\begin{array}{cccccccc} & \overbrace{\phantom{N_{11}N_{12}N_{13}}}^{3q_1^{(d)}-2 \ \ldots \ 3q_1^{(d)}} & & \overbrace{\phantom{N_{21}N_{22}N_{23}}}^{3q_2^{(d)}-2 \ \ldots \ 3q_2^{(d)}} & & \overbrace{\phantom{N_{31}N_{32}N_{33}}}^{3q_3^{(d)}-2 \ \ldots \ 3q_3^{(d)}} & \overbrace{\phantom{N_{41}N_{42}N_{43}}}^{3q_4^{(d)}-2 \ \ldots \ 3q_4^{(d)}} & \\ \ldots & N_{11}N_{12}N_{13} & \ldots & N_{21}N_{22}N_{23} & \ldots & N_{31}N_{32}N_{33} & N_{41}N_{42}N_{43} & \ldots \end{array} \right]$$

and again all other entries are zero.

6. Results

We begin by making some comparisons of our results with those given using the method described in Meylan (2002) where the FEM was used to find the modes for the plate and these modes we coupled to the water separately using a

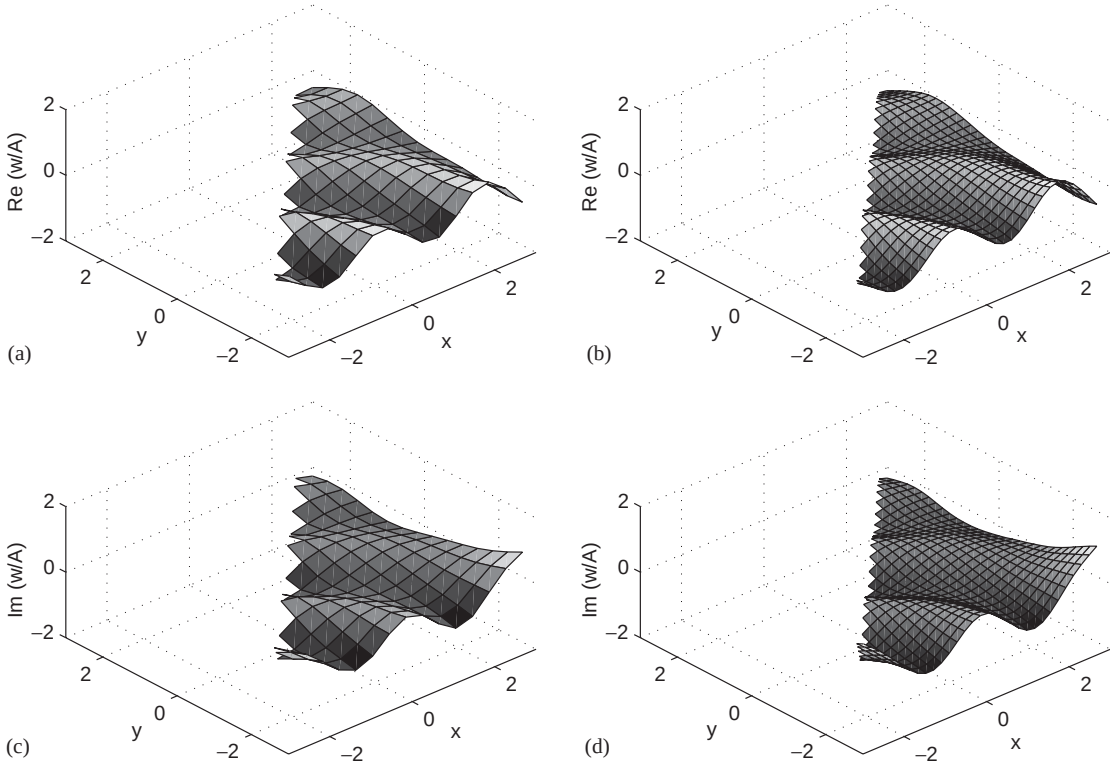

Fig. 5. As for Fig. 3 except for a geometry 2 plate.

Table 1
The error and time as a function of the number of panels for the higher-order method

Number of panels	Error	Time (s)
100	6.0633×10^{-4}	32.01
225	1.3738×10^{-4}	176.05
400	3.0189×10^{-5}	590.59
625	4.2498×10^{-6}	1617.83
900	0	3662.42

Table 2
The error and time as a function of the number of panels for the low-order method

Number of panels	Error	Time
100	1.3923×10^{-2}	5.80
400	1.0291×10^{-3}	76.36
900	3.6510×10^{-4}	353.39
1600	2.2060×10^{-4}	1904.11
2500	1.5050×10^{-4}	5832.23

Table 3
The errors as a function of the number of panels and the number of Gaussian integration points for the higher-order method

Number of panels	Error N, $M = 4$	Error N, $M = 6$	Error N, $M = 8$
100	6.0633×10^{-4}	4.3308×10^{-4}	3.2671×10^{-4}
400	3.0189×10^{-5}	2.1483×10^{-5}	1.6292×10^{-5}
900	2.8856×10^{-8}	4.3800×10^{-10}	0

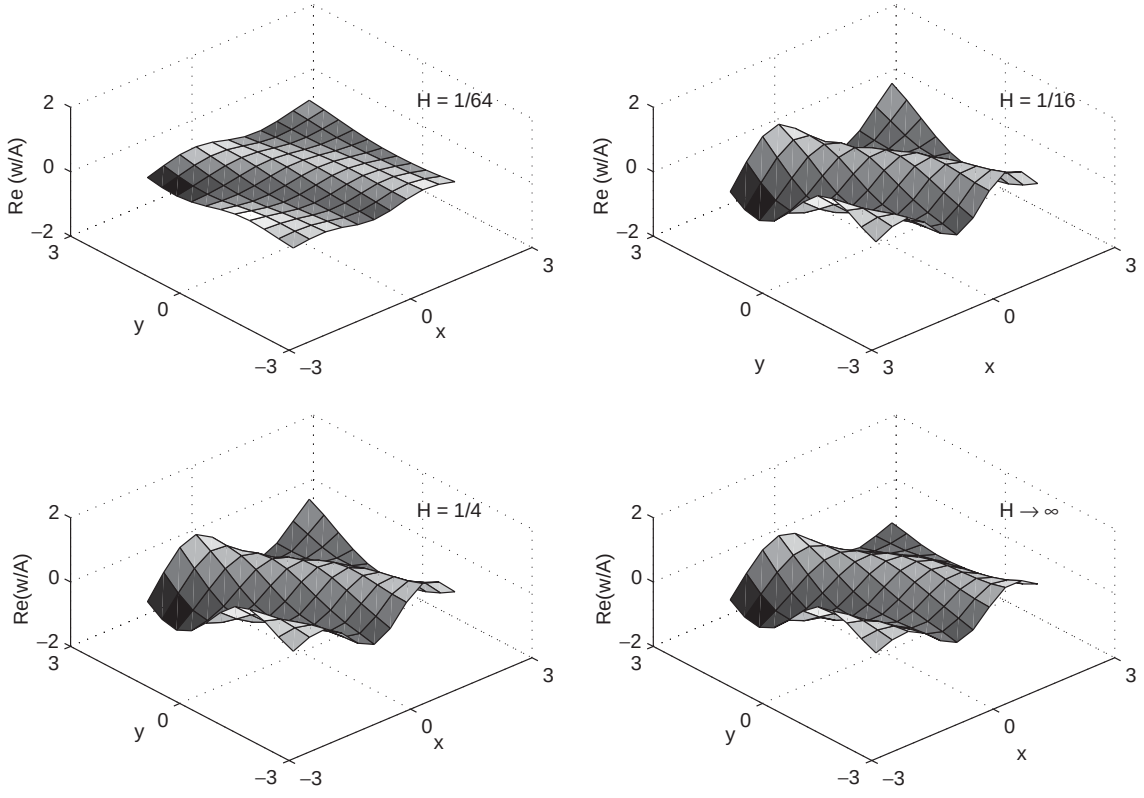

Fig. 6. The real part of the displacement for a geometry 1 plate using the higher-order method for water depth H as shown. The stiffness is $\beta = 0.01$ and the mass is $\gamma = 0$. The wavelength $\lambda = 2$ and the wave is incident from the $\theta = \pi/6$ direction.

constant panel (low-order) method. The numerical integration for Eq. (35) is carried out using the Gauss–Legendre Quadrature with $N = 4$ and $M = 4$, unless $d = e$ in which case we choose $M = 8$ so as to avoid the singularity in the Green function. Fig. 3 shows the comparison of the plate displacement w/A using our higher-order method and Meylan's low-order method for wavelength $\lambda = 2$, $\beta = 0.01$, and $\gamma = 0$. The direction of wave propagation is $\theta = \pi/6$

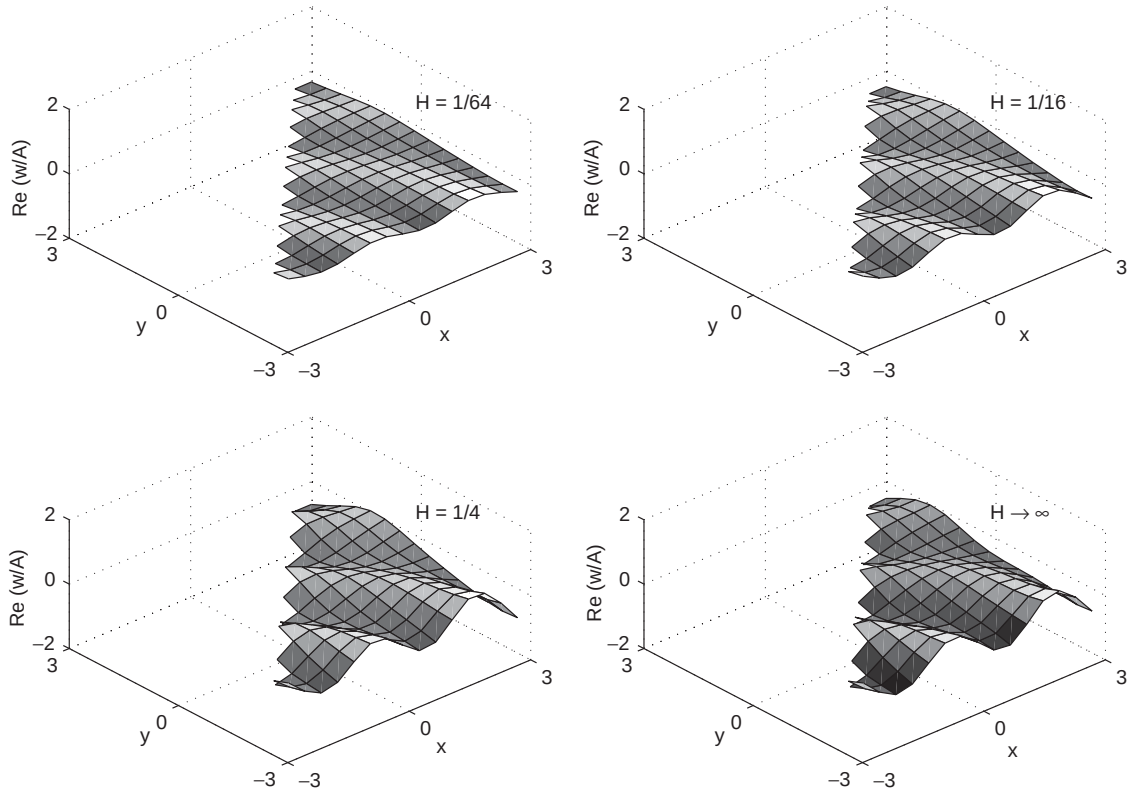

Fig. 7. As for Fig. 6 except for a geometry 2 plate.

and the water depth is infinite. The plate is square with side length 4 and area 16. This plate is geometry 1 shown in Fig. 4. The number of panels is 100 for the high-order method and 900 for the low-order method. Fig. 5 shows the same comparison for a triangular plate (geometry 2) also with area 16. The panel size is chosen to be equivalent to that used in Fig. 3. Both figures show the real and the imaginary part of the plate displacement and we can see that the two solutions agree.

We can make a more detailed comparison by comparing the error in the solutions. We compare the solutions for the geometry 1 plate and wave properties used in Fig. 3. Since we do not know the true solution we will compare all solutions to that obtained by the higher-order method with 900 panels. The error, E, between two solutions w_1 and w_2 will be given by the following expression:

$$E = \int_{\Delta} |w_1(\mathbf{x}) - w_2(\mathbf{x})|^2 \, \mathrm{d}\mathbf{x}.$$

We begin by comparing the higher-order method. Table 1 shows the convergence error for the number of panels being $100, 225, 400, 625$ and 900, respectively. The error for 900 panels is zero because this is the reference. The results show the good performance expected of the high-order method. Table 2 is a comparison of the convergence using the lower-order method of Meylan (2002). Comparing Tables 1 and 2 we see that the performance of the higher-order method is much better than the lower method as expected. We have also included the time data from the computations. While it is appropriate to compare the time data for the same method, it is not necessarily so appropriate to do so for two different methods. This is because we cannot be certain that the implementation of both methods is equally optimized. However, the time data shows that a significant extra cost is associated with the higher-order method.

Next, we make a comparison of the effect of increasing the number of Gaussian points used in the calculation of the higher-order solution. Table 3 shows the error for the number of Gaussian integration points per panel being 16 (M, $N = 4$), 25 (M, $N = 5$) and 36 (M, $N = 6$), respectively (unless $d = e$ in which case $M = 8$). The results are for $100, 400$ and 900 panels. The comparison is with the results for 36 integration points and 900 panels. These results show that very

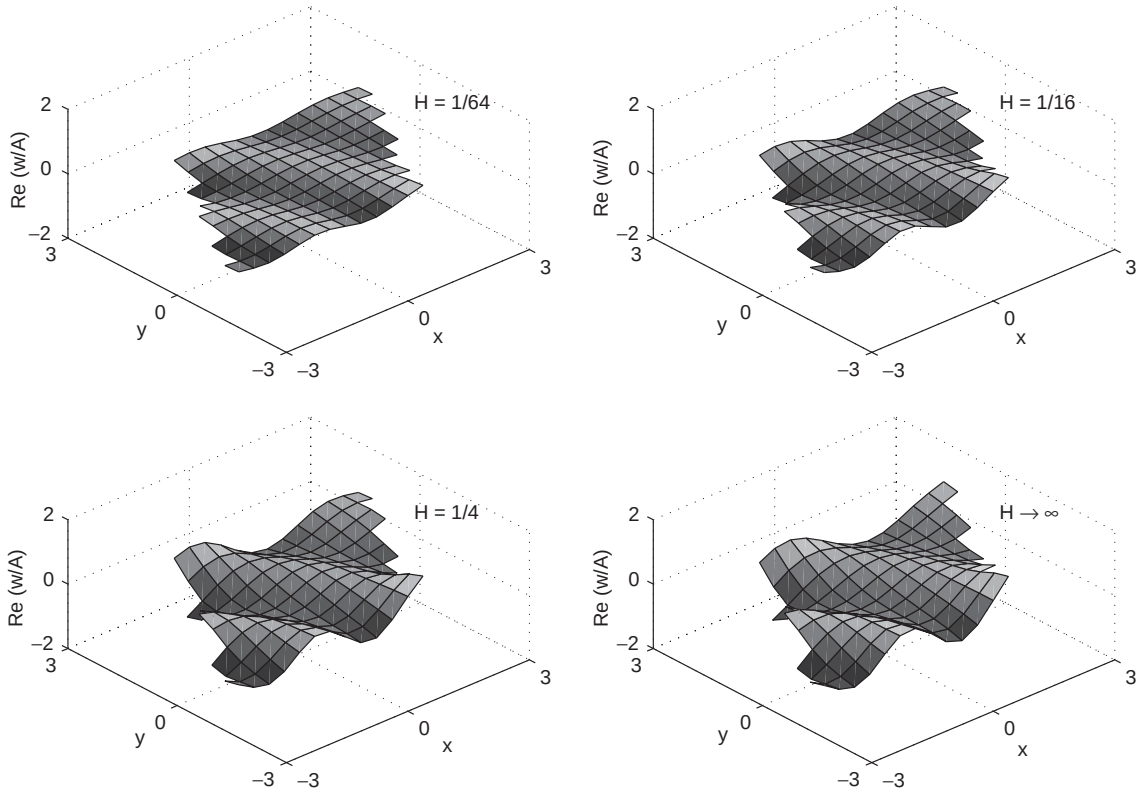

Fig. 8. As for Fig. 6 except for a geometry 3 plate.

little accuracy is gained by increasing the number of Gaussian points beyond 16. For brevity, we do not show results concerning increasing M in the case when $d = e$ and simply note that there was very little increase in the accuracy.

Fig. 6 shows the real part of the displacement for a geometry 1 plate with $\beta = 0.01$, $\gamma = 0$ and the direction of wave propagation is $\theta = \pi/6$ (exactly as in Fig. 3) for infinitely deep water and water of depth $H = 1/64$, $1/16$ and $1/4$. Since the changing water depth alters the wavelength for a fixed frequency we have chosen to keep the wavelength fixed so that the figures may be compared more meaningfully. The wavelength is $\lambda = 2$. Figs. 7–9 show the same situation as Fig. 6 except that plate geometries 2, 3 and 4 (which all have area 4) are chosen.

7. Summary

We have presented a solution for the wave-induced motion of a three-dimensional floating thin elastic plate of shallow draft. The solution involves solving two equations, the FEM equations for the plate and the BEM equations for the velocity potential of the water. Both of these equations were solved using the same higher-order representation of the displacement of the plate and the velocity potential of the water. From this discretization two equations were derived relating the displacement and potential which were solved simultaneously. The equation based on the FEM equations for the plate was similar to the standard FEM equations with a term due to the velocity potential for the water involving the mass matrix. The equation based on the BEM involved a matrix representation of the integral operator which is analogous to the mass and stiffness matrices used in the FEM.

Our results were compared with the known results given by Meylan (2002) and we also compared the performance of these two methods. The present, higher-order method, was shown to perform favourably in this comparison. We also investigated the effect of increasing the number of integration points on the convergence properties and found that good convergence was achieved with as few as 16 integration points per panel. Finally, we presented some displacement results for four different plate geometries.

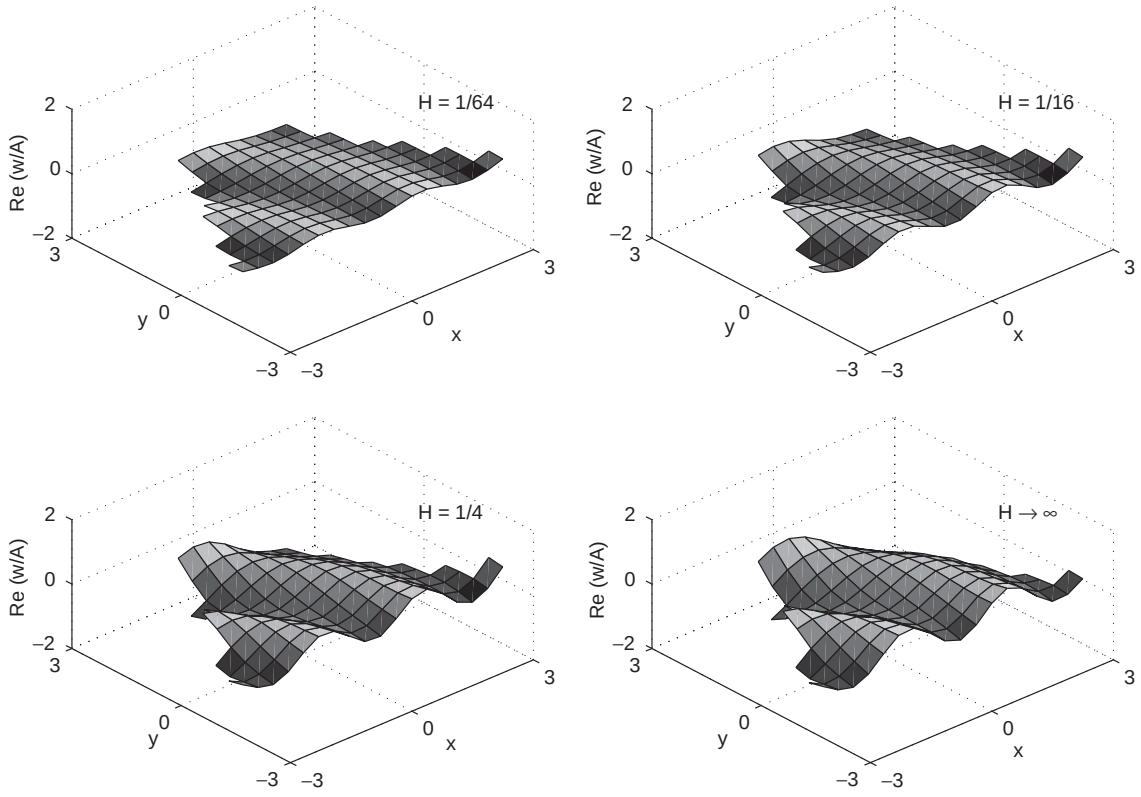

Fig. 9. As for Fig. 6 except for a geometry 4 plate.

Acknowledgements

This research was supported by the Marsden Grant UOO004.

References

Abramowitz, M., Stegun, I.A., 1970. Handbook of Mathematical Functions. Dover, New York.

Bishop, R.E.D., Price, W.G., Wu, Y., 1986. A general linear hydroelasticity theory of floating structures moving in a seaway. Philosophical Transactions of the Royal Society of London A 316, 375–426.

Hamamoto, T., Suzuki, A., Fujita, K., 1997. Hybrid dynamic analysis of large tension leg floating structures using plate elements. Proceedings of the Seventh International Offshore and Polar Engineering Conference, Hawaii, USA, Vol. 1, pp. 285–292.

Hermans, A.J., 2000. A boundary element method for the interaction of free-surface waves with a very large floating flexible platform. Journal of Fluids and Structures 14, 943–956.

Hildebrand, F.B., 1965. Methods of Applied Mathematics, 2nd Edition. Prentice-Hall, Englewood Cliffs, NJ.

John, F., 1950. On the motion of floating bodies II. Communications in Pure and Applied Mathematics 3, 45–101.

Kashiwagi, M., 1998. A b-spline Galerkin scheme for calculating hydroelastic response of a very large floating structure in waves. Journal of Marine Science and Technology 3, 37–49.

Kashiwagi, M., 2000. Research on hydroelastic response of vlfs: recent progress and future work. International Journal of Offshore and Polar Engineering 10 (2), 81–90.

Kim, W.D., 1965. On the harmonic oscillations of a rigid body on a free surface. Journal of Fluid Mechanics 21, 427–451.

Meylan, M.H., 2001. A variation equation for the wave forcing of floating thin plates. Journal of Applied Ocean Research 23 (4), 195–206.

Meylan, M.H., 2002. The wave response of ice floes of arbitrary geometry. Journal of Geophysical Research—Oceans 107 (C6) doi:10.1029/2000JC000713.

Meylan, M.H., Squire, V.A., 1994. The response of ice floes to ocean waves. Journal of Geophysical Research 99 (C1), 891–900.

Meylan, M.H., Squire, V.A., 1996. Response of a circular ice floe to ocean waves. Journal of Geophysical Research 101 (C4), 8869–8884.

Ohkusu, M., Namba, Y., 1998. Hydroelastic behaviour of a large floating platform of elongated form on head waves in shallow water. In: Kashiwagi, M., Koterayama, W., Ohkusu, M. (Eds.), Hydroelasticity in Marine Technology. Yomei Printing Cooperative Society. Fukuoka, Japan, pp. 177–184.

Petyt, M., 1990. Introduction to Finite Element Vibration Analysis. Cambridge University Press, Cambridge.

Squire, V.A., Duggan, J.P., Wadhams, P., Rottier, P.J., Liu, A.J., 1995. Of ocean waves and sea ice. Annual Review of Fluid Mechanics 27, 115–168.

Tayler, A.B., 1986. Mathematical Models in Applied Mathematics. Clarendon Press, Oxford.

Watanabe, E., Utsunomiya, T., Wang, C., 2004. Hydroelastic analysis of pontoon-type vlfs: a literature survey. Engineering Structures 26 (2), 245–256.

Wehausen, J., Laitone, E., 1960. Surface waves. In: Flügge, S., Truesdell, C. (Eds.), Fluid Dynamics III, Handbuch der Physik, Vol. 9. Springer, Berlin, pp. 446–778 (Chapter 3).

Yago, K., Endo, H., 1996. Model experiment and numerical calculation of the hydroelastic behavior of matlike vlfs. International Workshop of Very Large Floating Structures, pp. 209–216.

Yasuzawa, Y., Kagawa, K., Kawano, D., Kitabayashi, K., 1996. Wave response analysis of a flexible large floating structure. International Workshop of Very Large Floating Structures, pp. 221–228.